Nuclear Instruments and Methods in Physics Research A 654 (2011) 539–545

Contents lists available at ScienceDirect

Nuclear Instruments and Methods in Physics Research A

journal homepage: www.elsevier.com/locate/nima

Image quality phantom and parameters for high spatial resolution small-animal SPECT

Eric P. Visser [a,*], Anita A. Harteveld [b], Antoi P.W. Meeuwis [a], Jonathan A. Disselhorst [a], Freek J. Beekman [c,d], Wim J.G. Oyen [a], Otto C. Boerman [a]

[a] Department of Nuclear Medicine, Radboud University Nijmegen Medical Centre, Nijmegen, The Netherlands
[b] Institute for Technical Medicine, University of Twente, Enschede, The Netherlands
[c] Section of Radiation Detection and Medical Imaging, Delft University of Technology, Delft, The Netherlands
[d] Molecular Imaging Labs, Utrecht, The Netherlands

ARTICLE INFO

Article history:
Received 28 December 2010
Received in revised form
31 May 2011
Accepted 5 June 2011
Available online 24 June 2011

Keywords:
SPECT
Small animal
Image quality
NEMA
Phantom

ABSTRACT

At present, generally accepted standards to characterize small-animal single photon emission tomographs (SPECT) do not exist. Whereas for small-animal positron emission tomography (PET), the NEMA NU 4-2008 guidelines are available, such standards are still lacking for small-animal SPECT. More specifically, a dedicated image quality (IQ) phantom and corresponding IQ parameters are absent. The structures of the existing PET IQ phantom are too large to fully characterize the sub-millimeter spatial resolution of modern multi-pinhole SPECT scanners, and its diameter will not fit into all scanners when operating in high spatial resolution mode. We therefore designed and constructed an adapted IQ phantom with smaller internal structures and external diameter, and a facility to guarantee complete filling of the smallest rods. The associated IQ parameters were adapted from NEMA NU 4. An additional parameter, effective whole-body sensitivity, was defined since this was considered relevant in view of the variable size of the field of view and the use of multiple bed positions as encountered in modern small-animal SPECT scanners. The usefulness of the phantom was demonstrated for ^{99m}Tc in a USPECT-II scanner operated in whole-body scanning mode using a multi-pinhole mouse collimator with 0.6 mm pinhole diameter.

1. Introduction

Image quality (IQ) for whole-body, small-animal positron emission tomography (PET) or single photon emission computed tomography (SPECT) can be measured in a phantom that produces images simulating those obtained in a whole-body study of a small rodent with hot lesions, as well as uniform hot and some cold areas. For small-animal PET, a standard phantom with corresponding IQ parameters has been defined by the NEMA NU 4-2008 standards [1]. Fillable rods of different diameters are used to determine the activity recovery coefficients, which are indicative of the spatial resolution. The relative standard deviation in a uniform phantom region is a measure of the signal-to-noise ratio, while the overall uniformity in this region characterizes the attenuation and scatter correction performance. The activity measured in non-radioactive water- and air-filled compartments is indicative of the spill-over and scatter correction performance.

However, generally accepted standards to characterize small-animal SPECT scanners are lacking, and more specifically, a dedicated phantom with exactly defined IQ parameters does not exist. As far as we know, the scientific literature on IQ in small-animal SPECT is limited to qualitative demonstrations of the effective spatial resolution using Derenzo-like phantoms with hot or cold rods [2–8].

The existing NEMA NU 4 PET phantom (NU4IQ phantom), with smallest rod diameter of 1 mm, could be used in multi-pinhole, small-animal SPECT but its structures are too large to fully characterize the sub-millimeter spatial resolution that can be obtained using state-of-the-art scanners. In addition, its outer diameter of 33.5 mm may prevent the NU4IQ phantom to be used in collimators with small transaxial field of view (FOV) as optimal for imaging mice, the most widely used experimental animal. This holds true, e.g., for the USPECT-II mouse collimators in which whole-body scans are limited to 28 mm diameter [7], the GE Triumph X-SPECT when using small radii of rotation (adjustable between 15 and 175 mm), the Siemens Inveon SPECT using mouse collimators with 28 mm transaxial FOV, and the Bioscan NanoSpect using whole-body mouse collimators with 30 mm transaxial FOV (numbers for X-SPECT, Inveon SPECT and NanoSpect are from manufacturer's data sheets).

* Correspondence to: Department of Nuclear Medicine (444), Radboud University Nijmegen Medical Centre, P.O. Box 9101, 6500 HB Nijmegen, The Netherlands. Tel.: +31 24 3614081; fax: +31 24 3618942.
E-mail address: e.visser@nucmed.umcn.nl (E.P. Visser).

0168-9002/$ - see front matter © 2011 Elsevier B.V. All rights reserved.
doi:10.1016/j.nima.2011.06.036

The aim of the present work is to design, construct and test an adapted phantom (SPECTIQ phantom) with smaller internal structures and external diameter appropriate for IQ characterization of state-of-the-art high spatial resolution small-animal SPECT scanners. To this end, the NEMA NU 4-2008 IQ parameters have been redefined and extended to match the reduced phantom dimensions and the specific needs in high spatial resolution small-animal SPECT imaging. The use of the SPECTIQ phantom is demonstrated in the USPECT-II scanner for a 0.6 mm diameter multi-pinhole mouse collimator with 69 pinholes using ^{99m}Tc.

2. Methods

The NU4IQ phantom [1] is composed of a main phantom body, which contains a fillable cylindrical chamber with 30 mm diameter and 30 mm length, and a solid part of 20 mm length in which 5 fillable rods have been drilled through with diameters of 1, 2, 3, 4 and 5 mm. It further consists of a lid that attaches to the uniform region of the phantom and supports two cold region chambers. These regions are hollow cylinders of 15 mm length and 8 mm inner diameter with 1 mm wall thickness, and should be filled with non-radioactive water and air.

2.1. SPECTIQ phantom dimensions

Basically, the SPECTIQ phantom is a down-sized version of the NU4IQ phantom with a scaling factor of 0.7 for most of its dimensions. Scaling of the fillable rods, however, was chosen differently. In order to match the high spatial resolution of multi-pinhole SPECT scanners, the rod diameters have been down-sized to 0.35, 0.5, 0.75, 1.0 and 1.5 mm. Their length has been reduced from 20 to 6.5 mm, since micromachining poses limitations on the achievable drilling length of very thin cylindrical holes.

The total volume of the radioactive regions is 6.87 mL. The outer diameter and the length are 23.45 and 40 mm, respectively, leading to a total external phantom volume of 17.3 cm^3. The weight of the filled phantom is 19.2 g, which corresponds to a small mouse.

An overview of the dimensions of all structures of the SPECTIQ phantom is given in Table 1, in which the NU4IQ phantom dimensions have been included for comparison. A schematic drawing and a photograph of the SPECTIQ phantom are presented in Fig. 1. The phantom was constructed by Agile Engineering (Knoxville, TN, USA). According to the manufacturer, the tolerance of the dimensions is 0.005″ (0.127 mm), except for the fillable rods with 0.001″ (0.0254 mm) tolerance. The phantom material is polymethylmethacrylate (density = 1.19 g/cm^3). For practical reasons, an additional hole that can be sealed with a screw plug has been drilled through the removable bottom cover. This hole is positioned in line with the largest, 1.5 mm diameter fillable rod such that a syringe needle can be inserted into this hole and the rod to fill the main phantom compartment. Without this hole, complete filling of the small diameter rods with radioactive solution was not always feasible.

2.2. Definition of IQ parameters

The IQ parameters associated with the SPECTIQ phantom are taken from NEMA NU 4 with adaptations to account for the smaller dimensions. These parameters are (i) image noise, expressed as the percentage standard deviation (%STD$_{unif}$) in a central, cylindrical volume of interest over the center of the uniform region of the phantom, (ii) activity recovery coefficients for the filled rods (RC), expressed as the measured activity concentration in the rods divided by the mean phantom concentration, and (iii) spill-over ratios for the non-radioactive water- and air-filled compartments (SOR$_{wat}$, SOR$_{air}$), defined as the activity concentration measured in these compartments divided by the mean phantom concentration.

Table 1
Dimensions of the structures of the small-animal SPECT phantom (SPECTIQ) and the NEMA NU 4 image quality phantom (NU4IQ). All measures are in mm, unless otherwise specified.

	SPECTIQ phantom	NU4IQ phantom
Uniform body region		
Outer diameter	23.45	33.5
Inner diameter	21.0	30.0
Inner length	21.0	30.0
Wall thickness	1.225	1.75
Fillable rods		
Diameter 1	0.35	1.0
Diameter 2	0.50	2.0
Diameter 3	0.75	3.0
Diameter 4	1.0	4.0
Diameter 5	1.5	5.0
Length of rods	6.5	20.0
Distance between centers of rods and center of phantom (radius of circle on which rods are positioned)	4.9	7.0
Total radioactive volume (mL)	6.87	20.66
Non-radioactive compartments		
Inner diameter	5.6	8.0
Outer diameter	7.0	10.0
Outer length	10.5	15.0
Inner length	9.8	14.0
Wall thickness	0.7	1.0
Outer phantom dimensions		
Length	40.0	63.0
Diameter	23.45	33.5
External volume (cm^3)	17.3	55.5
Weight of filled phantom (g)	19.2	63.2

As for the NU4IQ phantom, the cylindrical region where %STD$_{unif}$ is determined corresponds to 75% of the active diameter and the central two-thirds of the active length, resulting in 15.75 and 7 mm, respectively. RC is determined using the central half of the length of the rods, that is, 3.25 mm. The transverse image pixel coordinates corresponding to the line profiles with maximum averaged activity concentration are determined according to Ref. [1], and RC is calculated as this concentration divided by the mean phantom concentration.

SOR$_{wat}$ and SOR$_{air}$ are calculated in cylindrical regions of half of the physical diameter and the central half of the outer length of the non-radioactive compartments, corresponding to 2.8 and 5.25 mm, respectively.

Standard deviations of RC are determined according to Ref. [1], that is

$$\%\mathrm{STD}_{\mathrm{RC}} = 100\sqrt{\left(\frac{\mathrm{STD}_{\text{line profile}}}{\mathrm{mean}_{\text{line profile}}}\right)^2 + \left(\frac{\mathrm{STD}_{\mathrm{unif}}}{\mathrm{mean}_{\mathrm{unif}}}\right)^2}$$

The standard deviations of SOR$_{wat}$ and SOR$_{air}$ are calculated in the same manner.

Although not prescribed by NEMA NU 4, a recovery-coefficient-to-noise ratio, defined as RCNR$_{rod}$ = 100(RC/%STD$_{RC}$), was determined since it can be a useful parameter to evaluate the trade-off between spatial resolution and activity recovery in small structures versus image noise. This additional parameter was determined for the smallest rod (0.35 mm diameter) for all image reconstruction settings.

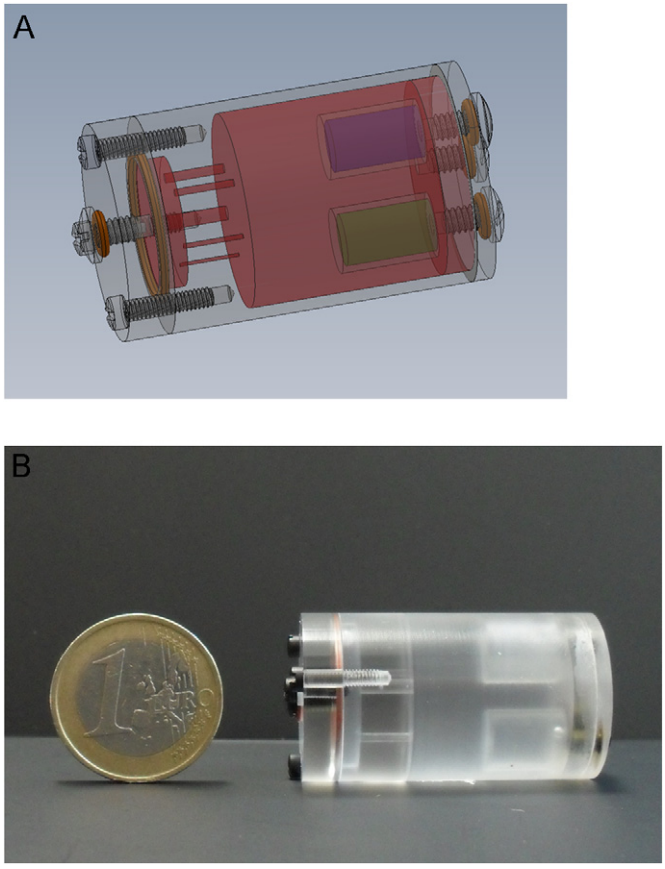

Fig. 1. (A) Schematic drawing of the SPECTIQ phantom. Regions to be filled with radioactive fluid are indicated in red. Cold water and air chambers are blue and green. For dimensions, see Table 1, (B) photograph of the phantom. (For interpretation of the references to color in this figure legend, the reader is referred to the web version of this article.)

2.3. Effective whole-body sensitivity

The SPECTIQ phantom allows to determine the effective whole-body sensitivity (EWBS), defined as the average photopeak count rate over a whole-body scan covering the phantom, divided by the average activity in the phantom during the scan (expressed, e.g., in counts per second (cps) per MBq ^{99m}Tc). We feel that in addition to centered point source sensitivity, as mostly specified by equipment manufacturers, EWBS can be a relevant parameter since the FOV of multi-pinhole SPECT scanners (as opposed to PET scanners) is in general not fixed. It depends, e.g., on the radii of rotation in case of rotating collimators and detectors, or on the bore size of cylindrical, static collimators. In order to obtain complete data, systems with rotating detectors require multiple detector angles at each bed position while systems with focused collimator geometries and stationary detectors may need more transaxial bed positions to expand the reconstructable FOV. Both procedures influence the time needed for whole-body acquisitions. Also in the axial direction, whole-body scans may require multiple bed positions[1] in which each bed position images part of the animal, and "sees" only part of its total activity. Larger animals will in general require more bed positions, thus decreasing effective sensitivity. This implies that for a proper comparison of the sensitivity of different scanners or different collimators, the total scanned volume and activity distribution should be standardized. The SPECTIQ phantom could serve as a standard. Moreover, an extended source such as the SPECTIQ phantom is expected to more realistically reflect the effects of scatter and attenuation as encountered in whole-body scans than does a centered point source.

[1] This can be achieved by step-wise horizontal bed motion, or by semi-continuous motion, resulting in "helical" scanning using rotating collimators.

2.4. Radionuclide, acquisition and reconstruction settings

The SPECTIQ phantom was filled with an aqueous solution of ^{99m}Tc, and scanned in the USPECT-II scanner [7] in whole-body, scanning focus mode using a mouse collimator with 0.6 mm diameter pinholes. Twenty-four consecutive scans of 1.0286 h duration each were made over of 24.69 h. Each of these scans consisted of 63 bed positions with overlapping FOVs to scan the whole phantom. Total data acquisition time per phantom scan was 1 h, the additional 0.0286 h is attributed to bed motion and the start-up time of the data acquisition for each new bed position.

Total activity and activity concentration at the start time of the data acquisition were 84.1 MBq and 12.2 MBq/mL, respectively. The activity was measured in a dose calibrator (Veenstra, VDC 404) with accuracy of $\pm 3\%$. This dose calibrator is regularly checked by the manufacturer using sources provided by North American Scientific Inc. that have been calibrated against standards at the Netherlands Metrology Institute (Nederlands Meetinstituut) and the German Federal Metrology Institute (Physikalisch-Technische Bundesanstalt). The average total phantom activity during the 24.69 h scan was 26.9 MBq. EWBS was determined using the measured counts per second in the photopeak window (as reported in the system's reconstruction log file) as a function of the decreasing phantom activity.

In order to obtain high count data, the list mode data over all 24 time frames were summed and reconstructed into a single image using the statistical iterative algorithm [9–11] as implemented in the USPECT-II system software version 34i3. The matrix size was $128 \times 128 \times 203$ voxels of 0.1875 mm in all directions, resulting in an image size of $24 \times 24 \times 38$ mm^3.

To demonstrate the usefulness of the SPECTIQ phantom for characterization or optimization of IQ parameters, we investigated the influence of the number of iterations, scatter correction and post-reconstruction spatial filtering on these parameters.

The number of iterations was varied between 1 and 12, the number of subsets was 16, the photopeak window was 126–154 keV, corresponding to a width of 20% of the peak energy (140 keV). The "scatter window" was 106–120 keV, which is half of the width of the photopeak window. Scatter correction has been performed using the multiple energy window method as described by Ogawa et al. [12], implemented in the USPECT-II vendor software. The effect of spatial filtering was demonstrated using no filtering, and a three-dimensional Gaussian filter with the kernel width of 0.6 mm full width at half maximum (FWHM), the theoretical lower limit for the geometrical spatial resolution using 0.6 mm diameter pinhole collimation [13].

3. Results

Fig. 2 shows cross-sections of the SPECTIQ phantom image reconstructed using 6 iterations, scatter correction and post-reconstruction filter (Gaussian, FWHM = 0.6 mm).

Fig. 3 shows RC for the ^{99m}Tc-filled rods of different diameters as a function of the number of iterations, with and without post-reconstruction filter. In Fig. 4, the results for $\%STD_{RC}$ for the smallest diameter (0.35 mm) rod and $\%STD_{unif}$ are presented. Fig. 5 shows $RCNR_{rod}$ for the two smallest diameter rods, again

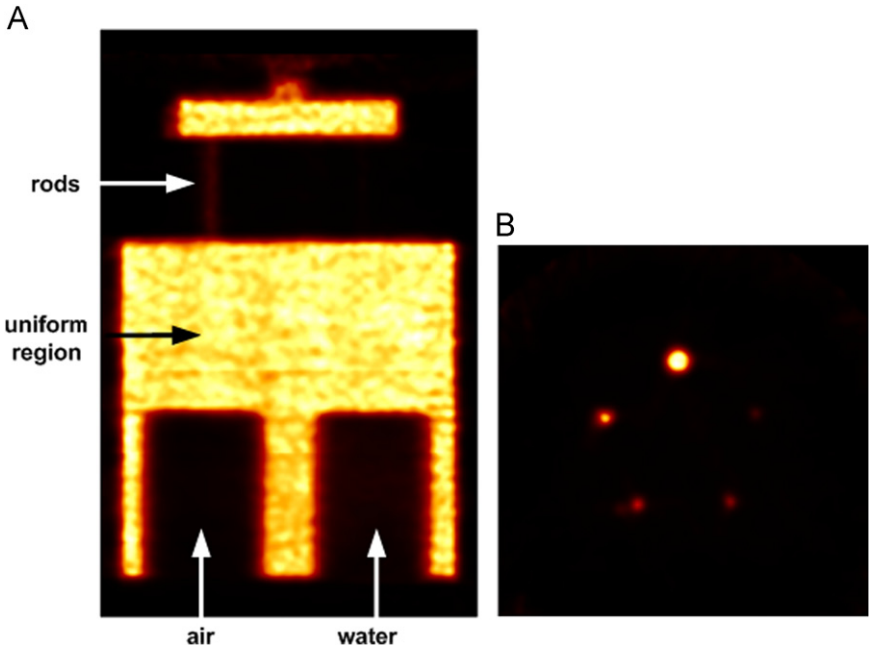

Fig. 2. Cross-sections of SPECTIQ phantom image reconstructed using 6 iterations, scatter correction and post-reconstruction filter (Gaussian, FWHM=0.6 mm). (A) Coronal cross-section showing the uniform phantom regions and the cold air- and water- filled chambers. (B) Transverse cross-section showing the filled rods.

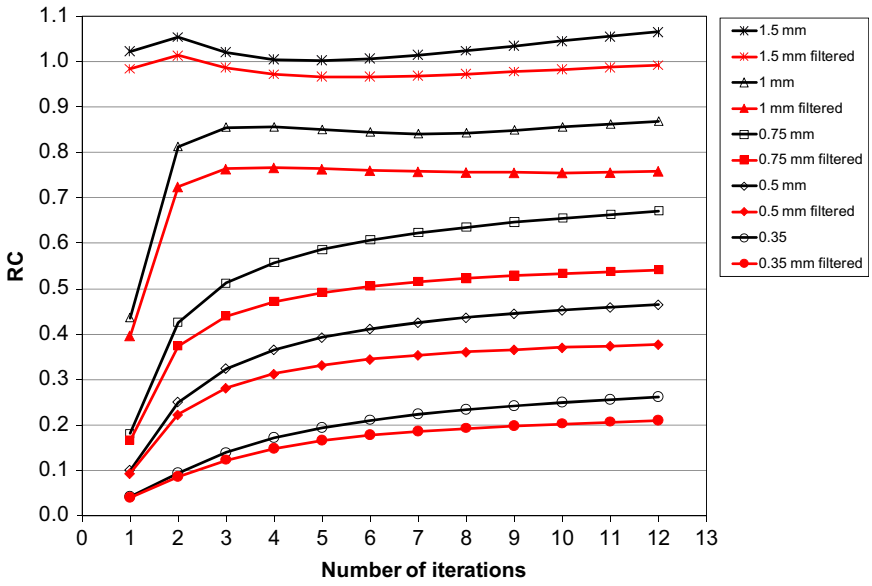

Fig. 3. RC for the ^{99m}Tc-filled rods of different diameters as a function of the number of iterations with and without post-reconstruction filter (Gaussian, FWHM=0.6 mm).

as a function of the number of iterations, with and without post-reconstruction filter.

SOR for the cold water and air chambers is shown in Fig. 6 as a function of the number of iterations, with and without scatter correction. Post-reconstruction filtering did not change the SOR values, accordingly the results are not shown. As observed in this figure, SOR_{wat} converges to constant values after approximately 8 iterations (≈ 0.074 and ≈ 0.071, without and with scatter correction, respectively), whereas SOR_{air} appears to decrease still after 12 iterations. It was therefore studied as to what extent SOR_{air} would further decrease on increasing the number of iterations. Without scatter correction, SOR_{air} converged to ≈ 0.030 at 16 iterations. With scatter correction it took 30 iterations to converge to ≈ 0.014.

Scatter correction was found to decrease the mean activity concentration in the uniform phantom region by $\approx 4.9\%$, independent of post-reconstruction filtering and the number of iterations. $\%STD_{unif}$ was not influenced by scatter correction, indicating that a possible increase due to noise in the scattered, lower energy photons was not observed given the present count statistics.

As shown in Fig. 7, the activity concentration in the ^{99m}Tc-filled rods obtained after 7 iterations did not change substantially by scatter correction. However, somewhat unexpectedly, convergence to the uncorrected values was slower using scatter correction, especially for the smallest rods (larger rods not shown for clarity). It should be noted that Fig. 7 presents activity concentrations, not RC. This was done to clearly separate the

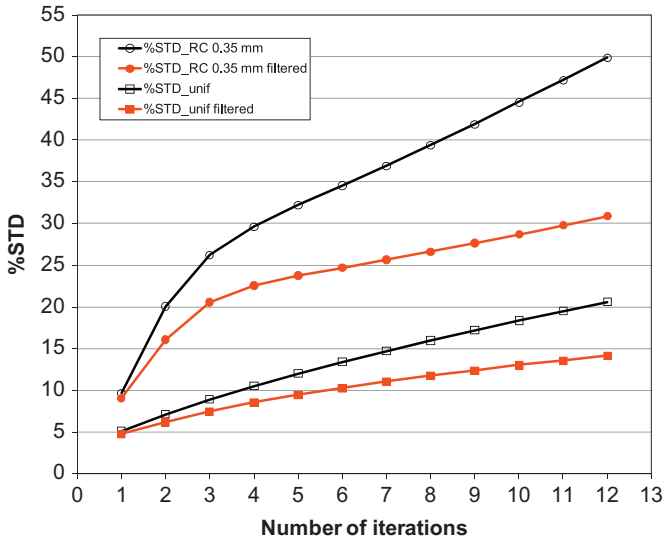

Fig. 4. % STD_{RC} for smallest ^{99m}Tc-filled rod (0.35 mm diameter), and %STD_{unif} as a function of the number of iterations with and without post-reconstruction filter (Gaussian, FWHM=0.6 mm).

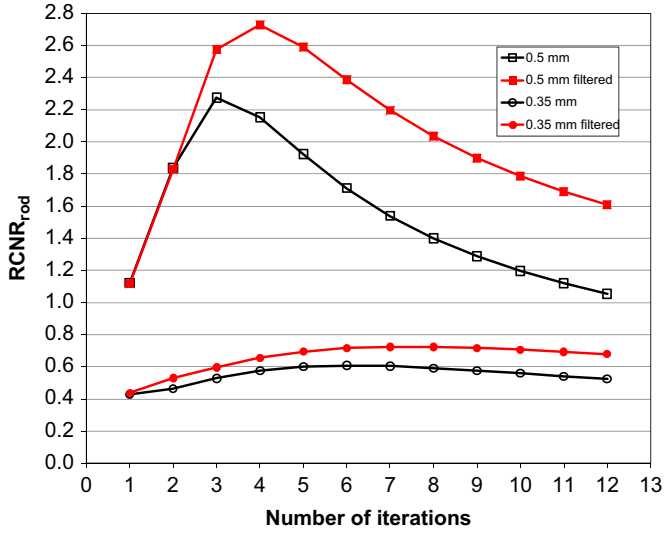

Fig. 5. $RCNR_{rod}$ for the two smallest ^{99m}Tc-filled rods (0.35 and 0.5 mm diameter) as a function of the number of iterations with and without post-reconstruction filter (Gaussian, FWHM=0.6 mm).

effect of scatter correction on the ^{99m}Tc-filled rods from the effect on the uniform phantom region. Since RC is the ratio of the corresponding activity concentrations, their values increased by ≈4.9% when using scatter correction.

Fig. 8 shows the measured photopeak counts per second, averaged for each time frame, as a function of the average ^{99m}Tc activity per time frame. The slope of the straight line directly yields EWBS=158 ± 5 cps/MBq. In view of the very large value of R^2=0.99995, the error in EWBS is essentially determined by the accuracy of 3% in the dose calibrator reading. The offset of the straight line of 143 cps corresponds to the average background activity in the photopeak window.

4. Discussion

The aim of this study was to introduce an IQ phantom and associated IQ parameters that can be used in state-of-the art, high

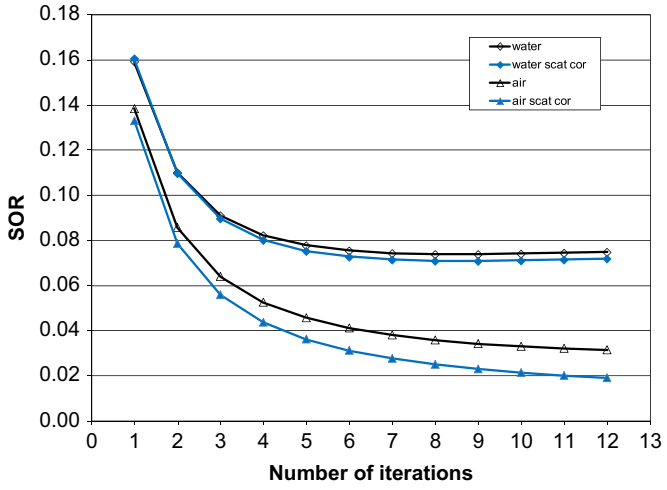

Fig. 6. SOR for the cold water and air chambers as a function of the number of iterations, with and without scatter correction.

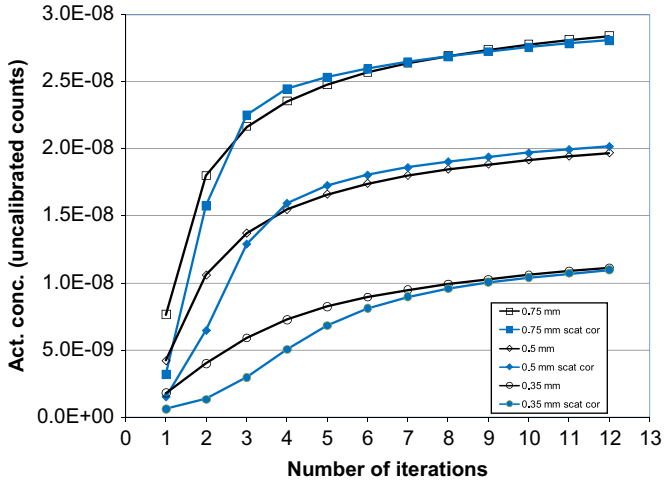

Fig. 7. Activity concentration in the 3 smallest ^{99m}TC-filled rods as a function of the number of iterations, with and without scatter correction. No spatial filter was used.

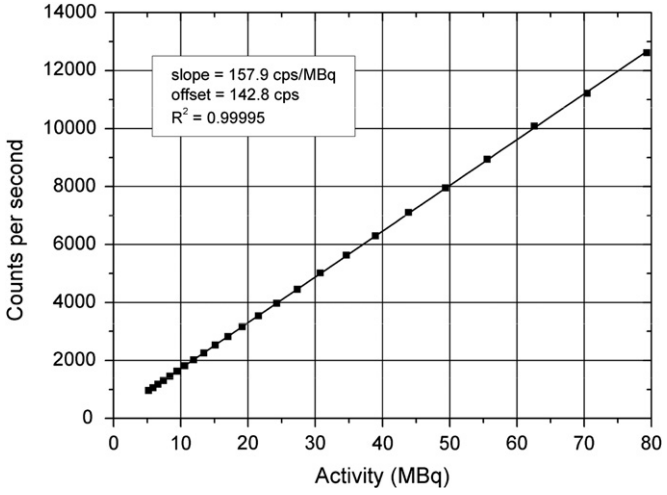

Fig. 8. Measured photopeak counts per second, averaged for each time frame, as a function of the average ^{99m}Tc activity per time frame.

spatial resolution small-animal SPECT scanners. The phantom can be used to compare the performance of different scanners in an objective, quantitative way for tasks representative for whole-body mouse imaging. Also, since most scanners can be equipped with different types of collimators, where a trade-off between spatial resolution and sensitivity depending on the pinhole diameter and the size of the FOV is involved, the phantom can be used to characterize these collimators and select the one that is most appropriate for the specific imaging goals.

Furthermore, also when the type of scanner and collimator are fixed, the user still has to define several acquisition and image reconstruction settings that will directly influence IQ. Among these are the injected activity, total scan time and scanned volume, number of iterations, spatial filtering and scatter and attenuation correction. The SPECTIQ phantom could serve as a useful aid to optimize these settings.

As for the NU4IQ phantom, recovery coefficients are based on hot rods in cold background. One could object that this would not be an ideal simulation of a lesion or organ in a real animal, since background activity will generally not be zero. However, this choice was motivated by the NEMA NU 4 taskforce since physical limitations prevent the production of hot spheres in non-zero background with physical walls much smaller than the spatial resolution of the imaging system. This holds true for small-animal PET, with spatial resolution of typically 1.5 mm FWHM [14], but it is *a forteriori* applicable to small-animal SPECT with even higher spatial resolution.

It was not the aim of this study to fully optimize all parameters that are available in the USPECT-II acquisition and reconstruction software. For this purpose, additional settings for the spatial filter, variation in the photopeak and scatter energy window width, scan duration and activity, attenuation correction, and different types of collimators, should have been investigated. Nevertheless, we feel that the limited number of parameters that have been varied clearly shows the way in which this could be dealt with. The well-known fact that using iterative reconstruction algorithms, a large number of iterations is necessary to recover small, active structures [15] was demonstrated in Fig. 3, which clearly shows the difference between the 1 and 1.5 mm diameter rods and the smaller ones. However, as a trade-off, image noise was increased by more iterations, as shown in Fig. 4. Spatial filtering can be used to decrease image noise. As shown in Fig. 5, the largest $RCNR_{rod}$ for the 0.35 mm diameter rod is obtained using 6 iterations without spatial filtering, and 8 iterations when using a Gaussian filter of 0.6 mm FWHM. The corresponding values for $RCNR_{rod}$ of 0.61 and 0.73 show that using more iterations combined with spatial filtering increases optimum $RCNR_{rod}$. Moreover, it is expected that the spatial filter width can still be optimized to further increase $RCNR_{rod}$. It is furthermore seen in this figure that larger structures (0.5 mm diameter rod) need fewer iterations to obtain maximum $RCNR_{rod}$.

Another phenomenon that was demonstrated is the strong decrease in SOR on increasing the number of iterations (Fig. 6), showing that cold regions in hot environments can only be recovered using many iterations, as has previously been described for PET image reconstruction [16]. It is further observed that SOR_{wat} is much larger than SOR_{air}, which is clearly attributed to the fact that photon scatter in water is stronger than in air. It is interesting to note the differences in scatter-related spill-over effects between SPECT and PET. Related to the detection of photon pairs forming lines of response (LOR) in PET, spill-over is to a large extent caused by scatter outside the cold compartments, causing the corresponding LORs to be falsely attributed to these compartments, independent of their density and scatter efficiency. This was observed in small-animal ^{18}F-PET [17], leading to almost equal values for SOR_{air} and SOR_{wat}. Because of single photon detection in SPECT, however, the activity measured in cold regions should ideally be proportional to the residual photon scatter originating in the cold region itself, which explains the observed difference between SOR_{air} and SOR_{wat}.

Theoretically, SOR_{air} should converge to almost 0 when using enough iterations and scatter correction. We investigated the possibility that the small residual value of ≈ 0.014 for SOR_{air}, as obtained after 30 iterations with scatter correction, could be attributed to background photons. For this purpose, a scan of 1 h duration with no activity in the FOV, and the mouse collimator mounted, was performed. Reconstruction of the list mode data in the ^{99m}Tc photopeak window led to activity concentrations of typically 20 times lower than measured in the air compartment of the SPECTIQ phantom. It is thus concluded that the contribution of background photons to SOR_{air} can be neglected. Since the residual SOR_{air} is very small, we did not further investigate this issue.

In summary, scatter correction had a positive effect on IQ since SOR decreased, whereas image noise and activity recovery did not deteriorate. However, when using scatter correction, convergence of the activity concentration in the small rods was slower than without scatter correction.

It is interesting to compare EWBS of 158 ± 5 cps/MBq with the single bed position, centered point source sensitivity of 1500 cps/MBq as presented in [7]. The difference between these values reflects the combined effect of photon attenuation and partial coverage of the total phantom activity in individual bed positions.

Finally, it should be mentioned that the SPECTIQ phantom was designed to simulate whole-body scans of a mouse, which in the USPECT-II scanner led to 63 bed positions to cover the external phantom volume. The relatively long duration of 24.69 h to obtain 24 consecutive whole-body scans with average activity of 26.9 MBq was chosen in order to obtain a "reasonable" image for all phantom regions, based on satisfactory count statistics. However, to simulate imaging of specific organs or tissues in restricted FOV, the structures in the SPECTIQ phantom could be scanned separately using single bed positions, and the scan duration could accordingly be shortened, or the activity be lowered while obtaining IQ parameters comparable to the present results.

5. Conclusion

An IQ phantom was presented for high spatial resolution small-animal SPECT. The usefulness of the phantom was demonstrated for the USPECT-II scanner using a 0.6 mm pinhole diameter mouse collimator. As far as we know, it will fit into all commercial small-animal SPECT scanners presently available when operated in whole-body mouse mode. The sizes of the phantom structures have been chosen to reflect the sub-millimeter spatial resolution of small-animal SPECT.

As stated before, the purpose of this study was not to compare scanners of different manufacturers, nor to fully optimize acquisition and reconstruction settings for different collimators or different radionuclides, and to demonstrate the effects in real animal scans. This should be the subject of future work. We feel, however, that the limited number of examples in this paper already demonstrates the way in which the phantom could be utilized to these goals. Finally, in view of the present lack of NEMA guidelines for small-animal SPECT, the SPECTIQ phantom and the associated IQ parameters could be the candidates for incorporation into future NEMA guidelines.

References

[1] NEMA, National Electrical Manufacturers Association, NEMA Standards Publication NU 4-2008. Rosslyn, VA, National Electrical Manufacturers Association, 2008.
[2] F.J. Beekman, F. van der Have, B. Vastenhouw, A.J. van der Linden, P.P. van Rijk, J.P. Burbach, M.P. Smidt, J. Nucl. Med. 46 (2005) 1194.

[3] F.P. Difilippo, Phys. Med. Biol. 53 (2008) 4185.
[4] S.D. Metzler, S. Vemulapalli, R.J. Jaszczak, G. Akabani, B.B. Chin, Mol. Imag. Biol. 12 (2010) 35.
[5] K. Ogawa, N. Ohmura, H. Iida, K. Nakamura, T. Nakahara, A. Kubo, Ann. Nucl. Med. 23 (2009) 763.
[6] N.U. Schramm, G. Ebel, U. Engeland, T. Schurrat, M. Behe, T.M. Behr, IEEE Trans. Nucl. Sci. NS-50 (2003) 315.
[7] F. van der Have, B. Vastenhouw, R.M. Ramakers, W. Branderhorst, J.O. Krah, C. Ji, S.G. Staelens, F.J. Beekman, J. Nucl. Med. 50 (2009) 599.
[8] C. Lackas, N.U. Schramm, J.W. Hoppin, U. Engeland, A. Wirrwar, H. Halling, IEEE Trans. Nucl. Sci. NS-52 (2005) 181.
[9] F. van der Have, B. Vastenhouw, M. Rentmeester, F.J. Beekman, IEEE Trans. Med. Imag. 27 (2008) 960.
[10] B. Vastenhouw, F. Beekman, J. Nucl. Med. 48 (2007) 487.
[11] W. Branderhorst, B. Vastenhouw, F.J. Beekman, Phys. Med. Biol. 55 (2010) 2023.
[12] K. Ogawa, Y. Harata, T. Ichihara, A. Kubo, S. Hashimoto, IEEE Trans. Med. Imag. 10 (1991) 408.
[13] S.R. Cherry, J.A. Sorenson, M.E. Phelps, Physics in Nuclear Medicine, Saunders/Elsevier Science, Philadelphia, PA, 2003.
[14] E.P. Visser, J.A. Disselhorst, M. Brom, P. Laverman, M. Gotthardt, W.J. Oyen, O.C. Boerman, J. Nucl. Med. 50 (2009) 139.
[15] J.W. Wallis, T.R. Miller, J. Nucl. Med. 34 (1993) 1793.
[16] R. Boellaard, A. van Lingen, A.A. Lammertsma, J. Nucl. Med. 42 (2001) 808.
[17] J.A. Disselhorst, M. Brom, P. Laverman, C.H. Slump, O.C. Boerman, W.J. Oyen, M. Gotthardt, E.P. Visser, J. Nucl. Med. 51 (2010) 610.